ACS APPLIED MATERIALS & INTERFACES

Research Article

www.acsami.org

# Hierarchically Porous Carbon Encapsulating Sulfur as a Superior Cathode Material for High Performance Lithium–Sulfur Batteries

Guiyin Xu, Bing Ding, Ping Nie, Laifa Shen, Hui Dou, and Xiaogang Zhang*

College of Materials Science & Engineering, Nanjing University of Aeronautics and Astronautics, Nanjing, 210016, P. R. China

*Supporting Information*

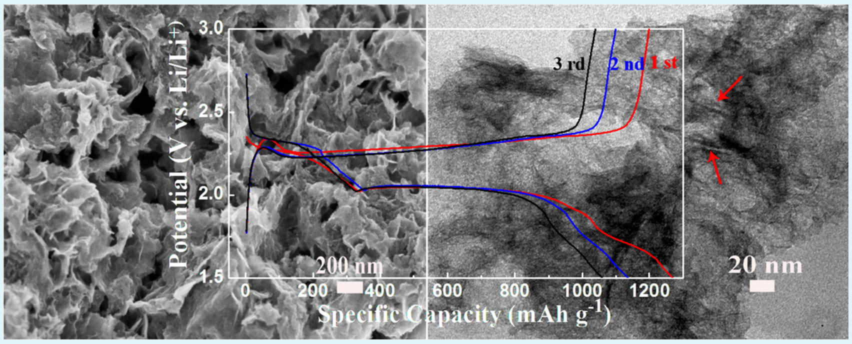

**ABSTRACT:** Lithium–sulfur (Li–S) batteries are deemed to be a promising energy storage device for next-generation high energy power system. However, insulation of S and dissolution of lithium polysulfides in the electrolyte lead to low utilization of sulfur and poor cycling performance, which seriously hamper the rapid development of Li–S batteries. Herein, we reported that encapsulating sulfur into hierarchically porous carbon (HPC) derived from the soluble starch with a template of needle-like nanosized $Mg(OH)_2$. HPC has a relatively high specific surface area of 902.5 $m^2\ g^{-1}$ and large total pore volume of 2.60 $cm^3\ g^{-1}$, resulting that a weight percent of sulfur in S/HPC is up to 84 wt %. When evaluated as cathodes for Li–S batteries, the S/HPC composite has a high discharge capacity of 1249 mAh $g^{-1}$ in the first cycle and a Coulombic efficiency as high as 94% with stable cycling over prolonged 100 charge/discharge cycles at a high current density of 1675 mA $g^{-1}$. The superior electrochemical performance of S/HPC is closely related to its unique structure, exhibiting the graphitic structure with a high developed porosity framework of macropores in combination with mesopores and micropores. Such nanostructure could shorten the transport pathway for both ions and electrons during prolonged cycling.

**KEYWORDS:** *lithium–sulfur batteries, hierarchical porous carbon, composite, cycling performance, high loading*

## INTRODUCTION

Rechargeable lithium–sulfur (Li–S) batteries have stirred a great deal of interest recently because of their high theoretical energy density of 2600 Wh $kg^{-1}$, assuming the complete reaction of Li and S to form $Li_2S$.[1−3] In addition, S is naturally abundant, inexpensive and nontoxic.[4] Therefore, Li–S batteries are considered to be a promising energy storage device for next-generation high energy power system.[5] Despite these considerable benefits in Li–S batteries, the practical application is still a formidable challenge.[6−9] First, sulfur is high electrically insulating, leading to low utilization of sulfur. Second, the high solubility of lithium polysulfides into the organic electrolyte can cause a loss of active cathode materials. In addition, an undesirable phenomenon generated during charge/discharge process, named the shuttle effect,[10] not only results in low Coulombic efficiency but also causes the serious lithium anode corrosion and loss of the active material. Moreover, further reduction of lithium polysulfides leads to the deposition of insulated $Li_2S$ onto the electrode surfaces. Finally, the cathode material suffers from the volume variation during charge/discharge process. All those undesirable factors give rise to severe capacity fading during extended cycling.

Various strategies to address the issues mentioned above have been explored.[11−14] Specially, carbonbased materials are paid much attention. They include carbon nanotube,[15,16] graphene,[17,18] graphene oxide/carbon nanotubes (GO/CNTs),[19,20] and so on.[21,22] The carbon framework can greatly facilitate electron transport. In addtion, the carbon hosts effectively contain sulfur and suppress the diffusion of polysulfides, meanwhile shorten the transport pathway for ions and improve the ability to withstand volume variation of the active material during prolonged cycling.[23,24] In our previous work, we reported that confining S into hierarchically porous carbon nanoplates (HPCN) derived from MOF-5.[25] The discharge capacity of HPCN/S is 1177 mAh $g^{-1}$ with stable cyclability and superior rate performance. The enhanced performance of the HPCN/S composite has close relation to its

**Received:** September 7, 2013
**Accepted:** December 17, 2013
**Published:** December 17, 2013

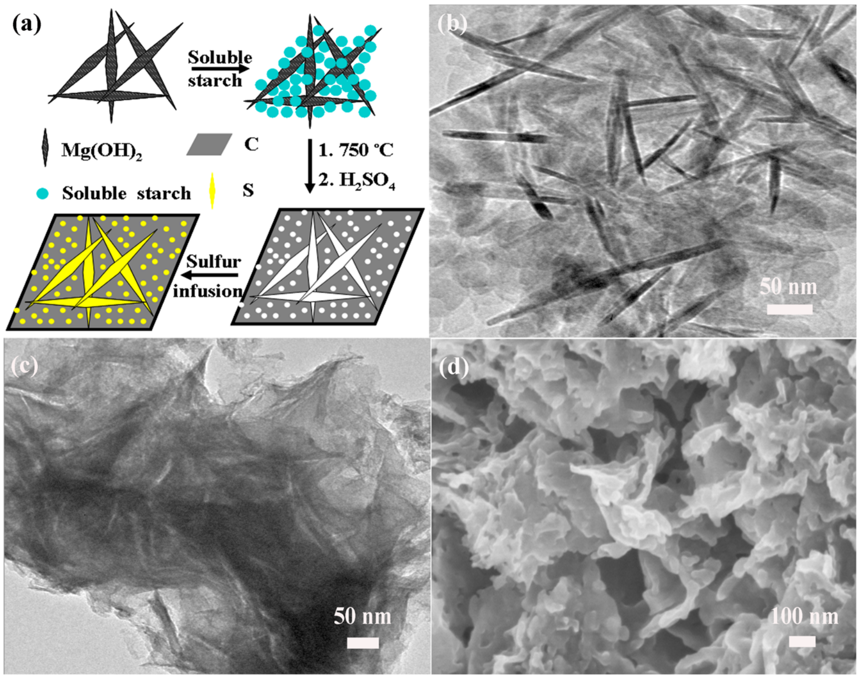

**Figure 1.** (a) Schematic illustration of the synthesis route for the S/HPC composite, (b) TEM image of needle-shaped $Mg(OH)_2$, (c) TEM, and (d) SEM image of HPC.

well-defined three-dimensional (3D) porosity plate nanostructure that not only provides stable ionic and electronic transfer pathway, but also plays the key role of retaining polysulfides and accommodating volume variation during prolonged cycling. However, *N*,*N*-dimethyformamide (DMF) used in the preparation of HPCN is not environmentally friendly and the unique structure of the hierarchically porous carbon for encapsulating sulfur needs to be further explored.

Herein, hierarchically porous carbon (HPC) has been synthesized by using the needle-shaped $Mg(OH)_2$ as the template and soluble starch as the raw material. The as-prepared HPC with a graphitic structure exhibits a high developed 3D porosity framework of macropores together with mesopores and micropores. These unique characteristics permit that HPC could act a promising host for confining S for high-performance Li−S batteries, namely the graphitic structure could enhance electric conductivity, macropores as ion-buffering reservoirs, mesopores and micropores for embedding the active material during charge/discharge process. The S/HPC composite exhibits excellent cycling stabilities and high specific capacities for Li storage, which clearly prove HPC with excellent conductivity, large surface area, unique pore-size distribution and low cost to be a promising material for high energy storage application.

## ■ EXPERIMENTAL SECTION

**Preparation of S/HPC Composite.** HPC was synthesized by using the needle-shaped $Mg(OH)_2$ as the template and soluble starch as the raw material.[26] One gram of $Mg(OH)_2$ in 10 mL of deionized water was dispersed for 1 h with ultrasonic stirring. Simultaneously, 1.0 g of soluble starch in 3 mL of deionized water was dispersed and was then mixed with the $Mg(OH)_2$ suspension with ultrasonic stirring for an extra 1 h. The as-obtained aqueous solutions were further dried under a vacuum atmosphere at 50 °C. Afterward, the dried mixture was heat-treated under $N_2$ in a tube furnace to 300 °C with a rate of 3 K $min^{-1}$, which was followed by further treatment to 400 °C with a heating rate of 1 K $min^{-1}$ and then 750 °C for 3 h with a rate of 3 K $min^{-1}$. Subsequently, it was immersed in 2 mol $L^{-1}$ sulfuric acid to remove MgO, and washed repeatedly with deionized water until neutral pH. Finally, the derived products were dried at 80 °C for 12 h under a vacuum atmosphere and HPC was obtained. To prepare the S/HPC composite, the mixture of HPC and element sulfur with the mass ratio of 15:85 were grinded in ethanol for 0.5 h and heat-treated at 155 °C for 10 h.

**Characterization.** Transmission electron microscopy (TEM) measurements, field emission scanning electron microscopy (FESEM), scanning transmission electronic microscope (STEM), and X-ray diffraction (XRD) patterns were carried out with FEI TECNAI-20, JEOL JSM-6380LV FE-SEM, Tecnai G2 F30, and Bruker-AXS D8 DISCOVER, respectively. The Raman spectra of HPC were measured with a 632.8 nm diode laser excitation on a 300 line S $mm^{-1}$ grating on a Jobin Yvon HR800 confocal Raman system at RT. The $N_2$ adsorption/desorption tests were performed by Brunauer−Emmett−Teller (BET) measurements on an ASAP-2010 surface area analyzer. Thermal gravimetric (TG) analysis was conducted under a $N_2$ atmosphere at a heating rate of 10 K $min^{-1}$ from 30 to 500 °C on a TG-DSC instrument (NETZSCH STA 409 PC).

**Electrochemical Characterization.** The working electrodes consisted of 70 wt % active material, 20 wt % conducting agent (acetylene black) and 10 wt % polyvinylidene fluoride (PVDF) binder with N-methyl pyrrolidinone (NMP) as dispersant. The cathode materials were prepared by a slurry coating procedure to uniformly spread on an aluminum foil as the current collector and dried at 70 °C for 12 h. Each current collector contained ∼1.0 mg $cm^{-2}$ active material. Electrochemical characterization of S/HPC was carried out by galvanostatic cycling in CR2016-type coin cells, which were assembled in an argon-filled glovebox with lithium metal as the anode and polypropylene (PP) film as the separator. The electrolyte was 1 mol $L^{-1}$ bis-(trifluoromethane) sulfonimide lithium (LiTFSI) and 0.1 mol $L^{-1}$ $LiNO_3$ in a mixture of 1, 2-dimethoxyethane (DME) and 1, 3-dioxolane (DOL) (1:1 by volume). Galvanostatic charged-discharge tests of the coin cells were conducted on a CT2001A cell test instrument (LAND Electronic Co.) at different current densities between the voltage window of 1.5 and 3.0 V (vs $Li/Li^+$). The cyclic voltammetry (CV) measurement was conducted with a CHI 600A electrochemical workstation between cutoff potentials of 1.0 to 3.0 V (vs $Li/Li^+$) at a scan rate of 0.5 mV $s^{-1}$. Electrochemical impedance

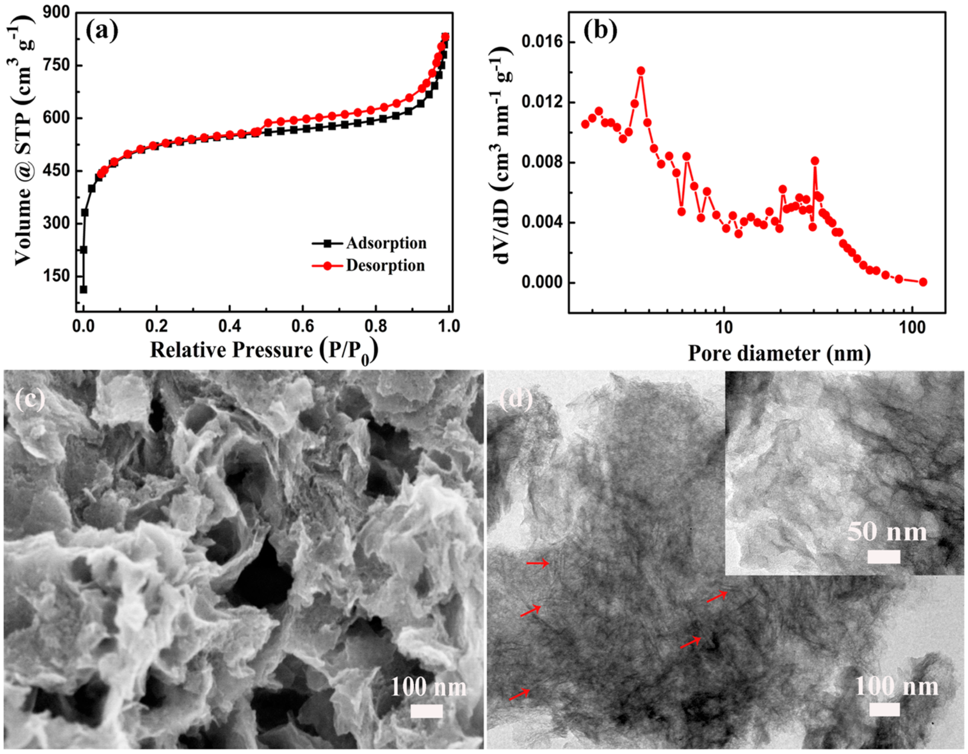

**Figure 2.** (a) $N_2$ adsorption/desorption isotherms at 77 K and (b) PSD of HPC(PSD derived from the desorption branch of the isotherms is calculated using the Barrett−Joyner−Halenda (BJH) method), (c) SEM, and (d) TEM images of S/HPC composite. (The arrows show the needle-like morphological feature and the inset is high-magnification TEM image in the edge of S/HPC.)

spectroscopy (EIS) was measured with an amplitude of 5 mV in the frequency range of 100 kHz−0.01 Hz.

## RESULTS AND DISCUSSION

The synthesis of HPC and the S/HPC composite is illustrated in Figure 1a. The needle-like nanosized $Mg(OH)_2$ (Figure 1b) is synthesized by the surfactant-mediated solution process. Owing to abundant nucleation centers of the obtained $Mg(OH)_2$, soluble starch can uniformly deposit on the surface of $Mg(OH)_2$ facilely.[27,28] In addition, when $Mg(OH)_2$ transforms to MgO between the temperature of 300−400 °C, the needle-shaped characteristic can still remain.[29] To copy the needle-like morphological feature better, soluble starch with the needle-shaped $Mg(OH)_2$ was heat-treated under $N_2$ between 300 and 400 °C with a heating rate of 1 K min$^{-1}$. As demonstrated in Figure 1c, the as-prepared HPC successfully copies the needle-like nanosized feature of $Mg(OH)_2$ and has abundant mesopores and macropores from the positions left by removing MgO. Simultaneously, the graphitic structures with abundant pores are formed, which result from the effect of the needle-like template (Figure 1d).[26] And the dense micropores come into being with the decomposition of soluble starch. HPC with graphitic structure (The graphitic structure can enhance the electric conductivity), which exhibits a hierarchically structured porosity network, is remarkably promising when employed for confining element sulfur as cathode materials for lithium−sulfur batteries.[30,31]

The $N_2$ adsorption/desorption isotherms and corresponding pore size distribution (PSD) curve for HPC are presented in Figure 2. A typical type I and type IV isotherms with a hysteresis loop are observed (Figure 2a).[32,33] It can be clearly seen that the isotherms show a sharp uptake at the low relative pressure ($P/P_0 < 0.1$), indicating the existence of abundant micropores. Significant hysteresis characteristics of the isotherms at high relative pressure can be seen ($P/P_0$ = 0.45−0.95) indicate that HPC is rich in mesopores. Subsequently, there is an obvious upward tendency at the high relative pressure ($P/P_0$ = 0.95−1.0), which may origin from the presence of macropores, offering abundant channels for liquid electrolyte. HPC exhibits a high developed hierarchical porosity framework of macropores together with mesopores and micropores, which corroborate well with the schematic illustration, TEM and SEM observation (Figure 1). The PSD data (Figure 2b) shows that the size of most of the pores is between 2 and 40 nm. Sulfur is embedded into these mesopores, which could effectively suppress the diffusion of polysulfides into the organic electrolyte. The hierarchically porous structure of HPC has a relatively high Brunauer−Emmett−Teller (BET) specific surface area of 902.5 m$^2$ g$^{-1}$ and large total pore volume of 2.60 cm$^3$ g$^{-1}$ (Supporting Information Table S1). Therefore, the S/HPC composite is a promising material as a superior cathode material for Li−S batteries. Macropores in HPC are beneficial for the permeability of the electrolyte and provide channels for the mass transport of Li ions. Micro/mesopores are good for buffering the volume change during lithiation and delithiation of sulfur and confining sulfur and polysulfides.

SEM and TEM are measured to observe the morphology of S/HPC. As displayed in Figure 2c, the S/HPC composite still remains the graphitic structure without any agglomerations of bulk sulfur on the surface of HPC, indicating the full incorporation of sulfur into the porous HPC hosts. Meanwhile, HPC and melted sulfur are both hydrophobic so that they have better compatibility. After the sulfur infusion process, the surface of HPC becomes smooth under the pressure of melted sulfur (Supporting Information, Figure S1a, b). The TEM

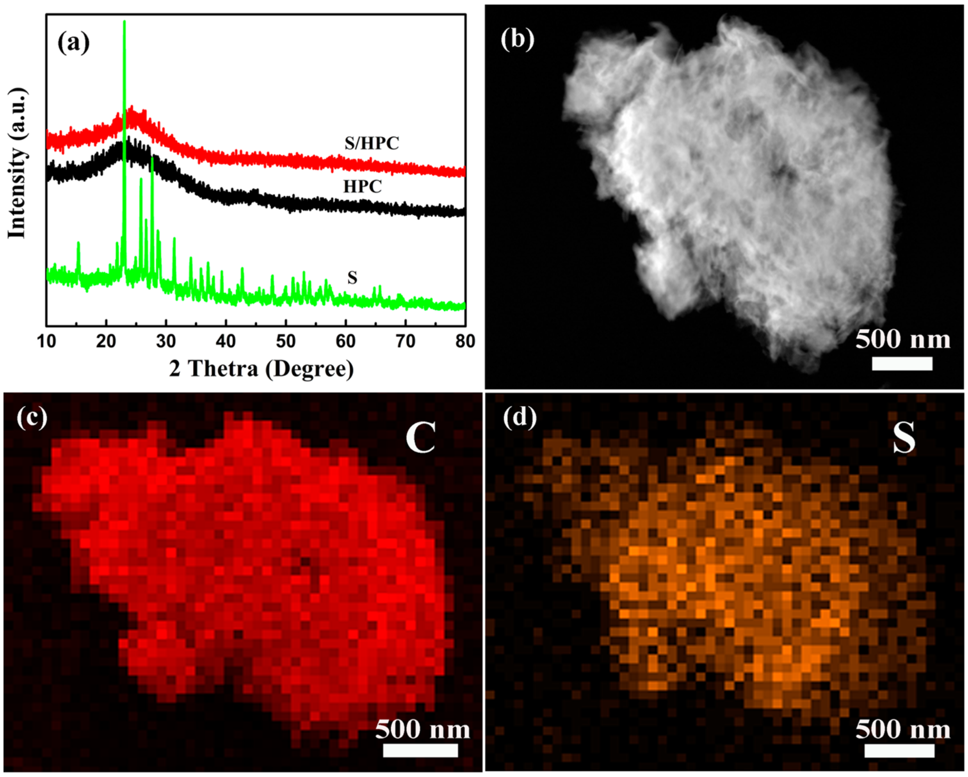

**Figure 3.** (a) XRD patterns of S, HPC, and S/HPC composite, (b) STEM image of S/HPC, and corresponding elemental mapping images of (c) carbon and (d) sulfur.

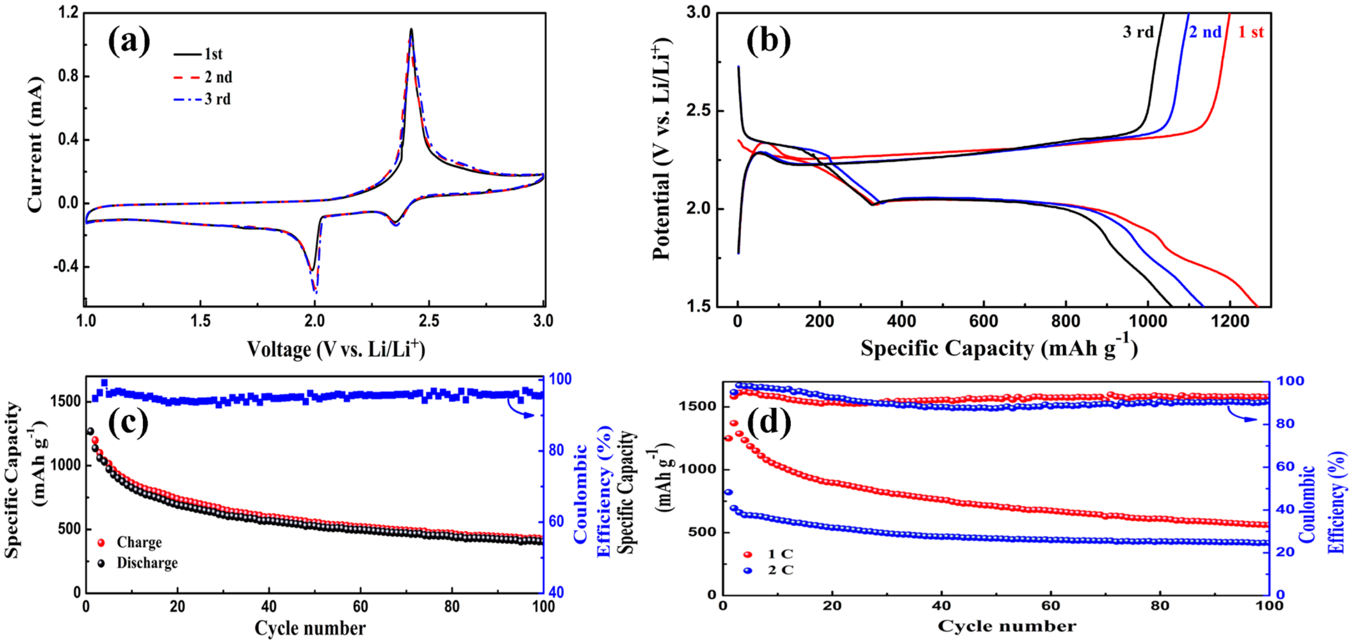

**Figure 4.** (a) Typical CV curves of S/HPC composite electrode at a scan rate of 0.5 mV $s^{-1}$. (b) Different cycles galvanostatic charge/discharge profiles of S/HPC composite electrode at 0.5 C. (c) Cycling performance of S/HPC composite electrode at a constant rate of 0.5 C. (d) Cycling performance of S/HPC composite electrode at a constant rate of 1 and 2 C.

image clearly illustrates that no large bulk sulfur could be observed in the S/HPC composite further demonstrating that sulfur homogeneously disperses in HPC (Figure 2d). The disordered graphitic layers on the edge of S/HPC shown in the inset of Figure 2d greatly enhance electron transport. The needle-like morphological feature remaining in S/HPC could effectively increase the reaction kinetics by shortening the transport pathway for both ions and electrons (The arrows show the needle-like morphological feature; Figure 2d and Supporting Information Figure S1c and d). After sulfur loading, the BET specific surface area (15.9 $m^2$ $g^{-1}$) and total pore volume (0.13 $cm^3$ $g^{-1}$) of S/HPC decrease markedly, accompanied by a significant reduction in the mesoporous region in PSD curve (Supporting Information Figure S2).

However, a portion of mesopores in S/HPC still remain, allowing the accessibility of the electrolyte and fast transport of lithium-ion during cycling.

To identify the distribution of sulfur in HPC, XRD and STEM are measured. The broad signals around 24° and 44° in the XRD pattern of HPC result mainly from amorphous carbon of HPC (Figure 3a).[25] These signals correspond to the (002) and (100) spacing of the graphene stacks, indicating that HPC has the typical structure of graphite structure (Supporting Information Figure S3). After sulfur is completely embedded into HPC, the entire disappearance of the diffraction peaks from crystalline sulfur demonstrates that sulfur has been successfully impregnated into the HPC matrix. The high dispersed S imbibed into the nanopores of HPC can generate intimate contact with conductive carbon framework, giving rise to a short pathway for transport of both lithium ions and electrons. The elemental mapping images of carbon and sulfur clearly demonstrate that sulfur has a highly dispersed state in HPC (Figure 3c, d), which corroborates well with the SEM, TEM and XRD observation.

Coin cell with the S/HPC cathode and a lithium foil anode was assembled to evaluate the electrochemical performance of S/HPC. Typical CV curves of the S/HPC composite electrode were tested in the potential window of 1.0−3.0 V at a scan rate of 0.5 mV $s^{-1}$ (Figure 4a). There is a typical characteristic of the oxidation and reduction of S in the CV curves.[34−36] The reduction peak at about 2.4 V can refer to the reduction of $S_8$ to high order lithium polysulfides ($Li_2S_x$, $4 \leq n \leq 8$). The strong cathodic peak at 2.0 V suggests a strong reduction of soluble polysulfide anions to $Li_2S_2/Li_2S$. In the following anodic scan, there is only one sharp oxidation peak at around 2.5 V, which is associated with the conversion of $Li_2S$ and $Li_2S_2$ to $Li_2S_8$. In the subsequent scans up to 3 cycles, there is no obvious change of the oxidation and reduction peak potentials, indicating good reactive reversibility and cycling stability of the S/HPC cathode.[37] Galvanostatic charge and discharge cycling of the Li−S batteries was conducted between cutoff potentials of 1.5 and 3.0 V at 0.5 C (1 C = 1675 mA $g^{-1}$, Figure 4b). The charge/discharge profiles of the S/HPC composite electrode show two distinct plateaus in the discharge curve and one plateau in the charge curve. Such charge/discharge profiles are typical for sulfur cathodes and consistent with previous reports.[38−40] The weight percent of sulfur in S/HPC is approximately up to 84 wt % (Supporting Information Figure S4), which agrees well with the theoretical value of loaded sulfur (Supporting Information Table S1). Therefore, the initial discharge capacity of S/HPC is 1269 mAh $g^{-1}$ (All of the capacities mentioned in this report are calculated based on the mass of active material sulfur, the loading of sulfur in the composite cathode is 58.8 wt %), which is close to double capacity of the sulfur cathode (667 mAh $g^{-1}$) in our previous report.[25] The discharge capacity is still up to 1060 mAh $g^{-1}$ after three cycles at the current density of 0.5 C. The excellent electrochemical performance of S/HPC has close relation to its unique structure mentioned above, which not only can provide stable transfer channels for ions and electrons, but also has the effect for improving the absorbent ability to confine lithium polysulfides and reduces their dissolution into the organic electrolyte during prolonged cycling.

At a constant current density of 0.5 C, the S/HPC composite shows a good cycling stability with a reversible capacity of 406 mAh $g^{-1}$ and a high Coulombic efficiency of 96% after 100 cycles (Figure 4c). The synergistic contribution from the graphite structure and hierarchically porous carbon of macropores in combination with micro/mesopores could shorten the transport pathway for ions and electrons to improve the reaction kinetics effectively, leading to a high capacity and superior rate performance. At a higher current density of 1 C, the S/HPC composite has a discharge capacity of 1249 mAh $g^{-1}$ in the first cycle and still remains 562 mAh $g^{-1}$ with a high Coulombic efficiency of 94% after 100 cycles. Even at a current density of 2 C, S/HPC still delivers a discharge capacity of 822 mAh $g^{-1}$ and remains 419 mAh $g^{-1}$ after 100 cycles (Figure 4d). The cycling performance of S/HPC electrode at a high constant rate is more stable. This can probably be attributed to the relatively rapid charge/discharge process at a high current density, where polysulfide ions are not immediately dissolved into the electrolyte with the adsorption effect of the micro/mesopores in HPC. The shuttle effect is suppressed so that the cycling performance of S/HPC can improve. And the capacity fades at high current rate bacause the complete utilization of the active material is limited.[25] Therefore, the stable anodic peak current and potential in the CV curves and the superior cycling performance of S/HPC electrode even at a high constant rate can confirm that the unique porous structure of HPC can effectively adsorb the active material and keep its structural integrity during the charge/discharge process.[25,37]

The characteristics of S/HPC cathode in Li−S batteries are elucidated by the schematic diagram (Scheme 1). The high specific capacity and superior rate capability of S/HPC are closely related to its unique structure, which favors both the ion and electron transportation in the Li−S batteries (Supporting Information Figure S5). First, the high surface area and large pore volume of HPC can load a high content of sulfur in the S/HPC composite so that the capacity can be increased. Second, the graphite structure in HPC greatly enhances electron transport, improving the utilization of the active material. Finally, the hierarchically porous structure in S/HPC can effectively adsorb the active material and suppress the shuttle effect, improving the cycling performance of S/HPC.[37] In addition, the porous structure remained in S/HPC would favor the infiltration of the organic electrolyte, high ion storage and rapid ion diffusion upon prolonged cycling.

**Scheme 1. Illustration of S/HPC Composite Cathode**

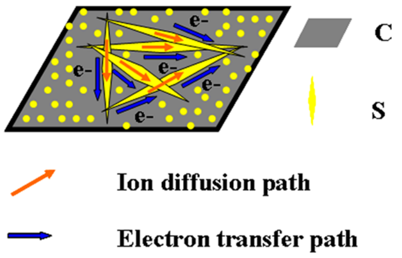

## CONCLUSIONS

In summary, we have successfully synthesized HPC with a graphitic structure, exhibiting a high developed hierarchical porosity framework of macropores together with mesopores and micropores. The graphitic structure can enhance electric conductivity and macropores as ion-buffering reservoirs could shorten ion diffusion distance. Simultaneously, mesopores and micropores can confine the active material upon repeated cycling. S/HPC is remarkably employed for confining S as a promising candidate for high-performance Li−S batteries. At a high current density of 1 C, the S/HPC composite has a discharge capacity of 1249 mAh $g^{-1}$ in the first cycle and a high Coulombic efficiency of 94% with stable cycling over prolonged 100 charge/discharge cycles. HPC may be applicable for other applications (such as catalyst supports, lithium ion batteries) due to its unique structure characteristic and high specific surface area. Based on this work, we will introduce other carbon sources, e.g. glucosamine for the nitrogen-doping, to further improve the conductivity of the composite material and obtain a better positive electrode material for Li−S batteries.

## ■ ASSOCIATED CONTENT

### Ⓢ Supporting Information

Supporting results mentioned in the text. This material is available free of charge via the Internet at http://pubs.acs.org.

## ■ AUTHOR INFORMATION

### Corresponding Author

*Tel.: +86-025-52112918. Fax: +86-025-52112626. E-mail: azhangxg@163.com.

### Notes

The authors declare no competing financial interest.

## ■ ACKNOWLEDGMENTS

The authors are grateful to the National Key Basic Research Program 973 (No. 2014CB239701), National Natural Science Foundation of China (No. 21103091, No. 21173120, No. 51372116), Natural Science Foundation of Jiangsu Province (No. BK2011030). G.Y.X. and B.D. gratefully acknowledge Funding of Graduate InnovationCenter in NUAA (No. kfjj120209), Outstanding Doctoral Dissertation in NUAA (BCXJ13-13) and Jiangsu Innovation Program for Graduate Education (CXZZ13_0158).

## ■ REFERENCES

(1) Ji, X. L.; Lee, K. T.; Nazar, L. F. *Nat. Mater.* **2009**, *8*, 500−506.

(2) Bruce, P. G.; Freunberger, S. A.; Hardwick, L. J.; Tarascon, J. M. *Nat. Mater.* **2012**, *11*, 19−29.

(3) Wang, H. L.; Yang, Y.; Liang, Y. Y.; Robinson, J. T.; Li, Y. G.; Jackson, A.; Cui, Y.; Dai, H. J. *Nano Lett.* **2011**, *11*, 2644−2647.

(4) Chung, W. J.; Griebel, J. J.; Kim, E. T.; Yoon, H.; Simmonds, A. G.; Ji, H. J.; Dirlam, P. T.; Glass, R. S.; Wie, J. J.; Nguyen, N. A.; Guralnick, B. W.; Park, J.; SomogyiÁrpád; Theato, P.; Mackay, M. E.; Sung, Y. E.; Char, K.; Pyun, J. *Nat. Chem.* **2013**, *5*, 518−524.

(5) Ji, X.; Evers, S.; Black, R.; Nazar, L. F. *Nat. Commun.* **2011**, *2*, 325.

(6) Xu, G. Y.; Ding, B.; Nie, P.; Shen, L. F.; Wang, J.; Zhang, X. G. *Chem.—Eur. J.* **2013**, *19*, 12306−12312.

(7) Lin, Z.; Liu, Z.; Dudney, N. J.; Liang, C. *ACS Nano* **2013**, DOI: 10.1021/nn400391h.

(8) Wei Seh, Z.; Li, W.; Cha, J. J.; Zheng, G.; Yang, Y.; McDowell, M. T.; Hsu, P. C.; Cui, Y. *Nat. Commun.* **2013**, *4*, 1331.

(9) Zhang, C.; Wu, H. B.; Yuan, C.; Guo, Z.; Lou, X. W. *Angew. Chem., Int. Ed.* **2012**, *124*, 9730−9733.

(10) Mikhaylik, Y. V.; Akridge, J. R. *J. Electrochem. Soc.* **2004**, *151*, A1969−A1976.

(11) Liang, C. D.; Dudney, N. J.; Howe, J. Y. *Chem. Mater.* **2009**, *21*, 4724−4730.

(12) Gao, J.; Lowe, M. A.; Kiya, Y.; Abruna, H. D. *J Phys Chem C* **2011**, *115*, 25132−25137.

(13) Yang, Y.; McDowell, M. T.; Jackson, A.; Cha, J. J.; Hong, S. S.; Cui, Y. *Nano Lett.* **2010**, *10*, 1486−1491.

(14) Yin, L.; Wang, J.; Lin, F.; Yang, J.; Nuli, Y. *Energy Environ. Sci.* **2012**, *5*, 6966−6972.

(15) Guo, J. C.; Xu, Y. H.; Wang, C. S. *Nano Lett.* **2011**, *11*, 4288−4294.

(16) Su, Y. S.; Fu, Y.; Manthiram, A. *Phys. Chem. Chem. Phys.* **2012**, *14*, 14495−14499.

(17) Ji, L. W.; Rao, M. M.; Zheng, H. M.; Zhang, L.; Li, Y. C.; Duan, W. H.; Guo, J. H.; Cairns, E. J.; Zhang, Y. G. *J. Am. Chem. Soc.* **2011**, *133*, 18522−18525.

(18) Ding, B.; Yuan, C.; Shen, L.; Xu, G.; Nie, P.; Lai, Q.; Zhang, X. *J. Mater. Chem. A* **2013**, *1*, 1096−1101.

(19) Xu, G. Y.; Ding, B.; Nie, P.; Luo, H. J.; Zhang, X. G. *Acta Phys. Chim. Sin.* **2013**, *29*, 546−552.

(20) Zhao, M. Q.; Liu, X. F.; Zhang, Q.; Tian, G. L.; Huang, J. Q.; Zhu, W. C.; Wei, F. *ACS Nano* **2012**, *6*, 10759−10769.

(21) Wang, D. W.; Zhou, G. M.; Li, F.; Wu, K. H.; Lu (Max), G. Q.; Cheng, H. M.; Gentle, I. R. *Phys. Chem. Chem. Phys.* **2012**, *14*, 8703−8710.

(22) Tao, X. Y.; Chen, X. R.; Xia, Y.; Huang, H.; Gan, Y. P.; Wu, R.; Chen, F.; Zhang, W. K. *J. Mater. Chem. A* **2013**, *1*, 3295−3301.

(23) Vu, A.; Qian, Y.; Stein, A. *Adv. Energy Mater.* **2012**, *2*, 1056−1085.

(24) Zhou, G.; Yin, L. C.; Wang, D. W.; Li, L.; Pei, S.; Gentle, I. R.; Li, F.; Cheng, H. M. *ACS Nano* **2013**, *7*, 5367−5375.

(25) Xu, G. Y.; Ding, B.; Shen, L. F.; Nie, P.; Han, J. P.; Zhang, X. G. *J. Mater. Chem. A* **2013**, *1*, 4490−4496.

(26) Zhang, W.; Huang, Z. H.; Cao, G.; Kang, F.; Yang, Y. *J. Power Sources* **2012**, *204*, 230−235.

(27) Qiu, L.; Xie, R.; Ding, P.; Qu, B. *Compos. Struct.* **2003**, *62*, 391−395.

(28) Zhang, W.; Huang, Z. H.; Zhou, C.; Cao, G.; Kang, F.; Yang, Y. *J. Mater. Chem.* **2012**, *22*, 7158−7163.

(29) Ding, Y.; Zhang, G.; Wu, H.; Hai, B.; Wang, L.; Qian, Y. *Chem. Mater.* **2001**, *13*, 435−440.

(30) Wang, D. W.; Li, F.; Liu, M.; Lu, G. Q.; Cheng, H. M. *Angew. Chem., Int. Ed.* **2008**, *120*, 379−382.

(31) Choi, N. S.; Chen, Z.; Freunberger, S. A.; Ji, X.; Sun, Y. K.; Amine, K.; Yushin, G.; Nazar, L. F.; Cho, J.; Bruce, P. G. *Angew. Chem., Int. Ed.* **2012**, *51*, 9994−10024.

(32) Su, Y. S.; Manthiram, A. *Nat. Commun.* **2012**, *3*, 1166.

(33) Fan, Z.; Liu, Y.; Yan, J.; Ning, G.; Wang, Q.; Wei, T.; Zhi, L.; Wei, F. *Adv. Energy Mater.* **2012**, *2*, 419−424.

(34) Barchasz, C.; Molton, F.; Duboc, C.; Leprêtre, J. C.; Patoux, S.; Alloin, F. *Anal. Chem.* **2012**, *84*, 3973−3980.

(35) Sun, F.; Wang, J.; Chen, H.; Li, W.; Qiao, W.; Long, D.; Ling, L. *ACS Appl. Mater. Interfaces* **2013**, *5*, 5630−5638.

(36) Zhou, G.; Wang, D. W.; Li, F.; Hou, P. X.; Yin, L.; Liu, C.; Lu, G. Q.; Gentle, I. R.; Cheng, H. M. *Energy Environ. Sci.* **2012**, *5*, 8901−8906.

(37) Zhang, B.; Qin, X.; Li, G. R.; Gao, X. P. *Energy Environ. Sci.* **2010**, *3*, 1531−1537.

(38) Ji, X. L.; Nazar, L. F. *J. Mater. Chem.* **2010**, *20*, 9821−9826.

(39) Wang, D.; Yu, Y.; Zhou, W.; Chen, H.; DiSalvo, F. J.; Muller, D. A.; Abruna, H. D. *Phys. Chem. Chem. Phys.* **2013**, *15*, 9051−9057.

(40) Ding, B.; Yuan, C.; Shen, L.; Xu, G.; Nie, P.; Zhang, X. *Chem.—Eur. J.* **2013**, *19*, 1013−1019.